BALLISTIC PERFORMANCE AND DAMAGE EVOLUTION OF TWARON CT 737 PARA-ARAMID COMPOSITE PANELS UNDER 9 × 19 MM FMJ LOADING

JINDRICH VILIS[1], ZDENEK POKORNY[1], JAN ZOUHAR[2], ROMAN VITEK[1], KAMIL PODANY[2], MARTIN DOSTAL[2], MARTIN KLIMES[1]

[1]University of Defence, Faculty of Military Technology, Kounicova 65, 662 10 Brno, Czech Republic

[2]Brno University of Technology, Faculty of Mechanical Engineering, Institute of Manufacturing Technology, Technicka 2896/2, 616 69 Brno, Czech Republic

DOI: 10.17973/MMSJ.2026_11_2026097

e-mail to corresponding author: jindrich.vilis@unob.cz

This study examines the mechanical behaviour and ballistic performance of Twaron CT 737 para-aramid/epoxy laminates manufactured by vacuum-assisted resin transfer moulding, with particular emphasis on damage development across different structural scales. Tensile, three-point flexural, and Shore D hardness tests were complemented by ballistic experiments using 9 × 19 mm full metal jacket (FMJ) ammunition. The composite achieved a mean tensile strength of 583.1 MPa, a flexural strength of 223.4 MPa, and a Shore D hardness of 87.9. A 24-layer panel with a nominal thickness of 14.2 mm prevented complete perforation during three consecutive impacts at a mean velocity of 399.3 m/s and a mean kinetic energy of 637.7 J. Scanning electron microscopy identified yarn pull-out, fibre fracture, fibrillation, and localized fibre–matrix separation, whereas X-ray computed tomography revealed internal deformation and interlaminar delamination extending through several reinforcement layers. These observations indicate that projectile arrest was accompanied by interacting fibre-scale and interlaminar damage processes within the woven architecture. The findings provide an experimental basis for understanding the ballistic response of multilayer para-aramid/epoxy composites under the investigated loading conditions.

KEYWORDS

Para-aramid composite, Twaron CT 737, ballistic resistance, 9 × 19 mm FMJ, multiscale damage evolution

1 INTRODUCTION

The increasing demand for lightweight yet highly efficient ballistic protection systems has accelerated the development of advanced textile-reinforced composite materials for modern defence and security applications [Girma Bekele 2026, Elgohary 2024, Ari 2025]. In contrast to conventional metallic armour systems, textile-based ballistic composites provide a favourable combination of low areal density, structural flexibility, and superior impact energy absorption capability during high-velocity projectile interaction [Titire 2025, Sharma 2021, Rubio 2019]. These characteristics are particularly important for modern personal protection systems, where weight reduction must be achieved without compromising ballistic resistance, operational mobility, or ergonomic comfort. Consequently, advanced composite structures reinforced with high-performance fibres have become an essential component of modern personal armour systems and multilayer protective structures.

Among currently available high-performance reinforcement materials, para-aramid fibres remain one of the most extensively utilized constituents of soft ballistic protection systems owing to their exceptional specific strength, thermal stability, high tensile modulus, and strain-rate-sensitive mechanical behaviour [Wang 2023, Stojanović 2024]. Consequently, woven para-aramid fabrics based on Twaron® and Kevlar® reinforcement systems are widely employed in personal body armour, impact-resistant structures, multilayer ballistic laminates, and hybrid protective systems [Kondor 2025, Shih 2022, Meliande 2023]. The ballistic efficiency of these woven structures originates not only from the intrinsic mechanical properties of the fibres, but also from complex interaction mechanisms occurring within the yarn architecture during projectile impact.

The ballistic response of woven aramid composites is governed by a multiscale interaction of deformation and failure mechanisms involving stress-wave propagation, yarn stretching, inter-yarn friction, transverse deformation, fibre rupture, fibrillation, yarn pull-out, and localized delamination within the woven architecture [Bilisik 2025, Kechagiadakis 2024, Chu 2024]. During ballistic impact, projectile kinetic energy is redistributed through rapid stress transfer between adjacent yarns and progressive activation of multiple energy dissipation mechanisms. The efficiency of these mechanisms strongly depends on projectile geometry, impact velocity, yarn architecture, fabric density, strain-rate-dependent material behaviour, and boundary conditions [Farias-Aguilar 2021, Viliš 2022]. Consequently, establishing direct relationships between multiscale damage evolution and ballistic energy dissipation remains a critical challenge in the design of lightweight protective systems.

Recent investigations have increasingly focused on multiscale characterization and numerical modelling of ballistic energy dissipation mechanisms in textile composite structures. Signetti et al. [Signetti 2020] demonstrated that penetration resistance of ballistic laminates is strongly governed by hierarchical stress redistribution mechanisms occurring from the fibre scale up to the laminate structure. Similarly, Nilakantan et al. [Nilakantan 2010] highlighted the importance of multiscale finite element modelling for understanding yarn-level interaction phenomena controlling impact resistance in woven ballistic fabrics. Recent studies further showed that hybrid UHMWPE/aramid structures significantly improve ballistic limit velocity and energy absorption capability through enhanced interfacial interaction and more efficient stress redistribution within the laminate architecture [Xu 2025, Peng 2024, Zhang 2024].

In addition to numerical and multiscale modelling approaches, increasing attention has recently been devoted to detailed post-impact damage characterization of para-aramid systems. SEM-based analyses of Twaron fibres revealed that fibrillation, fibre rupture, and progressive yarn pull-out represent the dominant mechanisms responsible for ballistic energy dissipation under dynamic loading conditions [Ceoromila 2025, Viliš 2023].

Despite substantial progress in the development of ballistic textile composites, detailed experimental investigations focused on the multiscale damage evolution of commercially available Twaron woven systems subjected to handgun ammunition impact remain relatively limited. In particular, the relationship between post-impact fractographic features and macroscopic ballistic response has not yet been sufficiently clarified for multilayer para-aramid composite architectures manufactured using VARTM technology. Therefore, the present study focuses on comprehensive experimental characterization of Twaron CT

737 composite panels subjected to 9 × 19 mm FMJ loading, combining mechanical testing, ballistic evaluation, SEM fractography, and X-ray computed tomography analysis.

2 MATERIAL AND EXPERIMENTAL PROCEDURES

2.1 *Investigated Reinforcement Material*

The investigated reinforcement material consisted of Twaron CT 737 para-aramid fabric supplied by Teijin Aramid for ballistic protection applications. The material consisted of a plain-woven para-aramid textile structure intended for lightweight multilayer ballistic systems and soft armour applications. The investigated fabric was supplied in multilayer textile form and subsequently used for preparation of composite specimens and ballistic targets.

According to the manufacturer's technical documentation, the fabric utilizes high-performance para-aramid yarns characterized by low density, high tensile resistance, and advantageous structural stability under dynamic loading conditions. Cross-sectional microstructural observations confirmed a compact woven architecture with relatively homogeneous yarn distribution and limited internal porosity, which is advantageous for stress redistribution during projectile impact interaction. Basic structural and physical properties of the investigated material are summarized in Table 1.

Property	Value
Material type	Para-aramid fabric
Manufacturer	Teijin Aramid
Weave architecture	Plain weave
Areal density	410 g/m^2
Thickness (single layer)	0.6 mm
Fibre density	1.44–1.45 g/cm^3

Table 1 Technical characteristics of Twaron CT 737 fabric

Following the evaluation of the basic structural parameters, the microstructure of the investigated Twaron CT 737 fabric was further examined using light microscopy. Cross-sectional and surface observations were performed using an Olympus DSX500 inverted optodigital microscope (Olympus, Japan).

2.2 *Fabrication of Composite Test Panels*

Composite panels reinforced with Twaron CT 737 fabric were manufactured using Vacuum-Assisted Resin Transfer Moulding (VARTM) technology, as shown in Figure 1. This manufacturing method was selected to facilitate resin infiltration into the woven reinforcement and reduce air entrapment during composite fabrication.



Figure 1 VARTM fabrication of Twaron CT 737 specimens

During fabrication, individual layers of Twaron CT 737 para-aramid reinforcement were arranged inside the mould cavity and sealed using a vacuum bagging system. The composite panels were impregnated with a two-component epoxy system consisting of LG 700 resin and HG 700 cycloaliphatic hardener (GRM Systems s.r.o., Czech Republic). According to the manufacturer's technical specifications, the viscosity of the LG 700 resin ranges from 500 to 700 mPa·s, while the HG 700 hardener exhibits a viscosity of 15–20 mPa·s. The components were mixed at a resin-to-hardener ratio of 100:30 by weight, following the manufacturer's recommendations. After vacuum stabilization, the epoxy mixture was introduced into the reinforcement architecture by vacuum-assisted infusion, facilitating resin infiltration between adjacent yarn bundles and impregnation of the woven para-aramid reinforcement.

Following impregnation, the manufactured laminates were initially cured at 22 °C for 20 h and subsequently stored under laboratory conditions at ambient temperature for several additional days before mechanical and ballistic testing. This additional conditioning period allowed further curing of the epoxy matrix. However, the degree of cure was not independently quantified.

Three laminate configurations were manufactured using the same VARTM process. The specimens intended for tensile testing consisted of six reinforcement layers with a nominal thickness of 2.5 mm, while the flexural specimens comprised eleven layers with a nominal thickness of 5.0 mm. The ballistic panels were manufactured from 24 reinforcement layers, resulting in a nominal thickness of approximately 14.2 mm. Their areal density was 15.1 kg/m², including both the para-aramid reinforcement and the epoxy matrix, with an average panel mass of approximately 1.4 kg. The different laminate thicknesses were selected according to the requirements of the respective experimental configurations.

Following fabrication and curing, the composite laminates were cut to the required specimen dimensions using abrasive waterjet cutting at an operating pressure of 380 MPa. Garnet abrasive with a particle size of 80 mesh was employed. The same cutting procedure was applied to both the mechanical test specimens and the ballistic panels.

2.3 Mechanical Testing Procedure

Mechanical characterization of the investigated Twaron CT 737/epoxy composite system included tensile testing, three-point flexural testing, and Shore D hardness measurements. The tensile and flexural specimens were prepared from the separately manufactured laminates described in Section 2.2. Seven specimens were tested for each mechanical test configuration (n = 7). The experimental results are expressed as the arithmetic mean ± standard deviation (SD), calculated from the individual measurements.

Tensile testing was performed using an Instron 5985 universal testing machine (Instron, USA) following the general testing procedure described in EN ISO 527-1. The specimens had nominal dimensions of 250 mm × 25 mm × 2.5 mm and were tested under displacement-controlled loading at a crosshead speed of 5 mm/min. The initial grip-to-grip distance was 115 mm. No extensometer was employed during tensile testing. Nominal tensile strain was calculated from the recorded crosshead displacement relative to the initial grip-to-grip distance of 115 mm. Tensile strength was determined from the maximum recorded force and the initial cross-sectional area of each specimen. The apparent tensile modulus was evaluated by linear regression of the nominal stress–strain response within the initial strain interval of 0.10–0.30%. This interval was selected to characterize the initial tensile stiffness of the composite. Since strain was derived from crosshead displacement rather than measured directly on the specimen, the resulting modulus may include contributions from machine compliance and deformation within the gripping system.

Flexural properties were evaluated using a Zwick Z100 testing machine (ZwickRoell, Germany) by three-point bending based on EN ISO 178. The specimens had nominal dimensions of 80 mm × 15 mm × 5 mm, and the support span was set to 64 mm. The tests were performed under displacement-controlled loading at a crosshead speed of 2 mm/min.

In addition, Shore D hardness measurements were performed according to EN ISO 868 using a Shore DIGI-Test II hardness tester to evaluate the surface resistance of the composite panels against localized indentation loading.

2.4 Ballistic Impact Testing

Ballistic impact experiments were conducted using a laboratory testing station equipped with a universal breech, ballistic barrel, optoelectronic velocity gates, radar-based velocity measurement system, and high-speed camera. The investigated Twaron CT 737 composite panel, with nominal dimensions of 300 × 300 mm and a thickness of 14.2 mm, was positioned at a shooting distance of 5 m. The experimental arrangement is illustrated in Figure 2. Projectile velocities were measured using optoelectronic gates and additionally monitored by radar, while high-speed imaging was employed to record the dynamic interaction between the projectile and the composite structure.

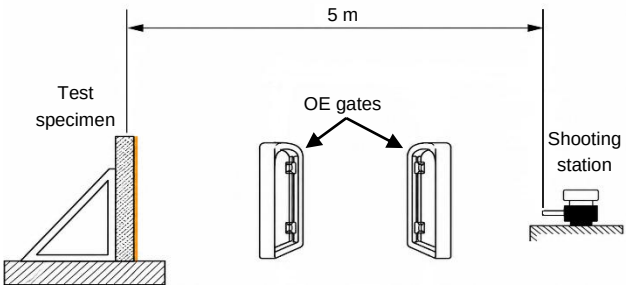


Figure 2 Experimental arrangement of the ballistic testing station, including the shooting system, optoelectronic velocity gates, and composite target positioned at a distance of 5 m

The experiments were performed using 9 × 19 mm full metal jacket (FMJ) ammunition with a nominal projectile mass of 8.0 g. The test conditions were selected with reference to the 9 mm FMJ round-nose threat specified for Level II in NIJ Standard 0101.06, particularly its nominal reference velocity of 398 m/s. The standard was used to define the reference projectile characteristics and impact velocity rather than to reproduce the complete qualification procedure.

During testing, the composite panel was positioned between rigid support frames and secured using eight bolts distributed around its perimeter. The panel was clamped along all four edges, providing a fixed peripheral support condition. No backing material was placed behind the panel, allowing its rear surface to deform without direct support from an additional medium. Three consecutive shots were applied to spatially separated locations on the same panel, following a predefined firing sequence.

The experimental procedure was designed to evaluate resistance to complete perforation and document the associated dynamic response and post-impact damage. The adopted mounting configuration differed from the standardized NIJ backing arrangement, and backface deformation was not quantitatively assessed. Consequently, the experiments represent a controlled ballistic evaluation of the investigated composite configuration rather than a complete NIJ Level II qualification test.

2.5 Post-Impact Analysis

Following ballistic testing, the impacted specimens were subjected to detailed microstructural and fractographic analyses aimed at identifying the dominant deformation and failure mechanisms responsible for ballistic energy dissipation within the woven architecture. The analyses focused primarily on fibre fibrillation, yarn pull-out, localized delamination, transverse yarn deformation, matrix cracking, and progressive fibre rupture induced during projectile impact.

Microstructural and fracture surface observations were performed using a TESCAN MIRA4 scanning electron microscope (TESCAN, Czech Republic).

In addition, internal structural damage and penetration-induced deformation were investigated using X-ray computed tomography (CT) performed with a TESCAN UniTOM XL system (TESCAN, Czech Republic).

3 RESULTS

3.1 Woven Architecture and Microstructural Features of Twaron CT 737

Cross-sectional microstructural observations of the investigated Twaron CT 737/epoxy composite are presented in Figure 3.

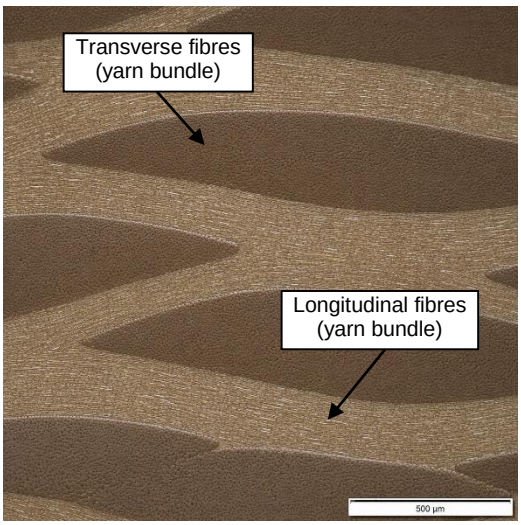


Figure 3 Woven architecture of Twaron CT 737 (150×)

Figure 3 presents an optical micrograph of the polished cross-section of the Twaron CT 737/epoxy composite. The microstructure reveals alternating regions corresponding to longitudinally and transversely oriented para-aramid yarn bundles. The darker regions represent transversely oriented yarn bundles, whereas the lighter, textured regions correspond to longitudinally oriented yarn bundles. Their alternating arrangement reflects the characteristic interlaced geometry of the plain-weave reinforcement architecture. The epoxy matrix occupies the spaces between individual fibres and adjacent yarn bundles, contributing to the cohesion of the composite structure.

Higher-magnification microstructural observations are presented in Figure 4.

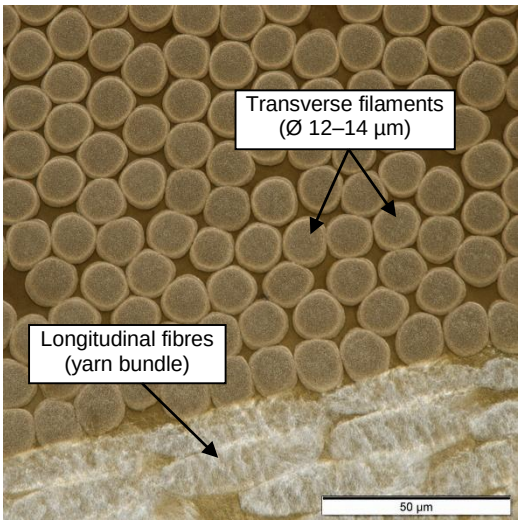


Figure 4 Para-aramid microstructure and reinforcement–matrix interface (2,000×)

Figure 4 provides a detailed view of the para-aramid filament cross-sections and the reinforcement–matrix interface. The darker, predominantly circular regions correspond to transversely oriented para-aramid filaments arranged in closely packed bundles, whereas the lighter, elongated structures in the lower part of the micrograph represent longitudinally oriented fibres. The filament diameters, measured using an Olympus DSX500 optodigital microscope, ranged from approximately 12 to 14 µm. The epoxy matrix occupies the spaces between adjacent filaments, forming a distinct fibre–matrix interface. No extensive interfacial separation was observed within the investigated field of view, indicating structural continuity at the observed interface, although localized defects elsewhere in the composite cannot be excluded.

3.2 Mechanical Properties of Twaron Composite Specimens

The mechanical properties of the investigated Twaron CT 737/epoxy composites were evaluated under tensile and three-point flexural loading conditions. Seven specimens were tested for each loading configuration, and three experimental curves were selected for graphical presentation to illustrate the characteristic deformation behaviour while maintaining figure clarity.

The tensile stress–strain responses of the selected specimens are presented in Figure 5.

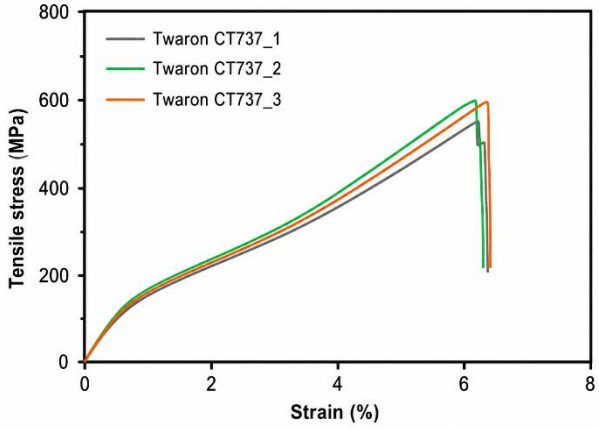


Figure 5 Representative tensile stress–strain curves of three selected Twaron CT 737/epoxy composite specimens

As shown in Figure 5, the tensile stress–strain responses exhibited an initially nonlinear region followed by a progressive increase in stress towards the maximum loading point. Following the maximum stress, a rapid decrease in load-bearing capacity was observed, indicating substantial structural damage and failure of the reinforcement architecture. The presented curves illustrate the characteristic tensile behaviour of three selected specimens, while the statistical evaluation of all seven measurements is provided in Table 2.

The flexural stress–deformation responses are presented in Figure 6.

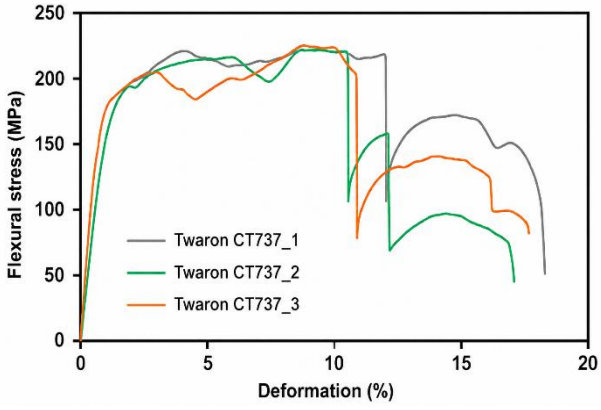


Figure 6 Representative three-point flexural stress–deformation curves of three selected Twaron CT 737/epoxy composite specimens

As illustrated in Figure 6, the flexural response was characterized by pronounced nonlinear deformation and progressive changes in load-bearing capacity. Following the initial maximum, successive reductions and partial recovery of the recorded stress were observed, indicating progressive damage development during bending. Compared with tensile loading, the flexural response exhibited a more gradual loss of load-bearing capacity.

The three representative curves illustrate the characteristic flexural behaviour, whereas the statistical results obtained from all seven specimens are summarized in Table 2.

The mechanical properties of the investigated composite specimens are summarized in Table 2 as arithmetic means and standard deviations obtained from seven individual measurements per loading configuration (n = 7).

Property	Value
Tensile strength	583.1 ± 16.2 MPa
Apparent tensile modulus	17.2 ± 0.8 GPa
Maximum tensile strain	6.2 ± 0.1%
Flexural strength	223.4 ± 6.3 MPa
Flexural modulus	18.1 ± 0.7 GPa
Shore D hardness	87.9 ± 1.1

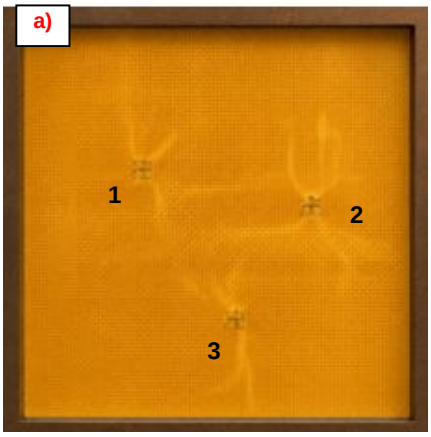
Table 2 Average mechanical properties of Twaron CT 737/epoxy composite specimens (reported mean ± SD, n = 7)

The mechanical results indicate distinct deformation and failure characteristics under tensile and flexural loading. Tensile loading resulted in a relatively rapid reduction in load-bearing capacity after the maximum stress, whereas flexural loading produced progressive stress reductions and partial load recovery.

3.3 *Ballistic Resistance against 9 × 19 mm FMJ Ammunition*

The ballistic resistance of the Twaron CT 737 composite panel was evaluated under three consecutive impacts with 9 × 19 mm full metal jacket (FMJ) projectiles. Figure 7 presents the front and rear surfaces of the panel after ballistic loading, with the individual impact locations numbered according to the firing sequence. The first projectile impacted the upper-left region, the second the upper-right region, and the third the lower-central region of the panel. The measured centre-to-centre distances between the impact locations were approximately 95–117 mm, while the distances from the impact centres to the nearest panel edges were approximately 87–101 mm.

The front surface (Figure 7a) exhibits three distinct impact locations characterized by localized damage to the woven para-aramid reinforcement. The rear surface (Figure 7b) shows localized out-of-plane deformation associated with the projectile impacts. The visible surface damage remained concentrated around the individual impact locations.



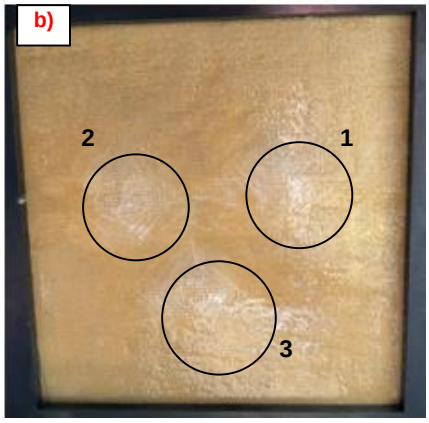


Figure 7 Front and rear surfaces of the Twaron CT 737 composite panel after three consecutive ballistic impacts: (a) front (strike) surface; (b) rear surface; impact locations are numbered according to the firing sequence

The investigated composite panel prevented complete perforation during all three ballistic impacts. The mean impact velocity was 399.3 m/s, corresponding to a mean kinetic energy of 637.7 J. The individual impact parameters are summarized in Table 3.

Shot number	Projectile weight (g)	Impact velocity (m/s)	Impact kinetic energy (J)	Perforation
1	8.0	403.7	651.9	No
2		395.0	624.1	
3		399.1	637.1	

Table 3 Ballistic impact parameters of Twaron CT 737 composite panel

The dynamic interaction between the projectile and the composite panel was recorded using a high-speed camera system. The corresponding image sequence is presented in Figure 8.

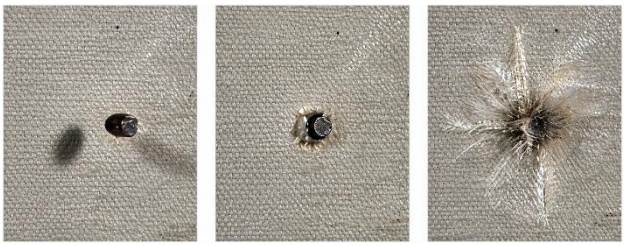


Figure 8 High-speed camera sequence illustrating the interaction between a 9 × 19 mm FMJ projectile and the Twaron CT 737 composite panel

As shown in Figure 8, the projectile impact induced rapid localized deformation of the woven para-aramid reinforcement. The deformation initially developed within the impact region and subsequently propagated into the surrounding composite structure.

3.4 *Multiscale Damage Mechanisms under Ballistic Impact*

Post-impact examination revealed localized damage concentrated within the primary projectile interaction regions. The macroscopic damage morphology observed after ballistic loading is presented in Figure 9.

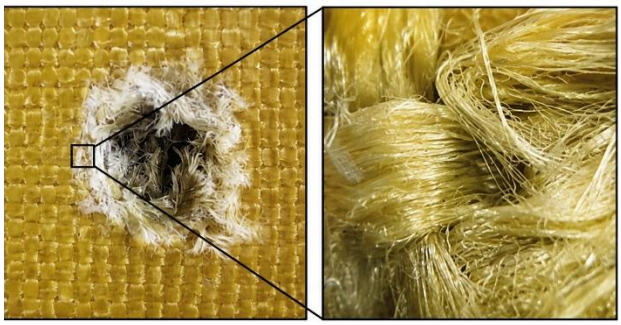


Figure 9 Macroscopic morphology of the projectile impact region showing localized damage and deformation of the woven para-aramid reinforcement

The frontal impact regions exhibited pronounced deformation of the woven para-aramid architecture in the vicinity of the projectile trajectories. Optical observations revealed localized yarn distortion, structural compaction, and partial extraction of yarn bundles from the surrounding matrix-rich regions. Damage was predominantly concentrated within the impact zones, while the surrounding reinforcement architecture retained its overall structural continuity. No complete projectile perforation or catastrophic structural failure of the composite panel was observed.

Fractographic examination using scanning electron microscopy (SEM) revealed several characteristic microscale damage mechanisms associated with projectile impact. As illustrated in Figure 10, the primary damage regions exhibited extensive yarn pull-out accompanied by progressive fracture of para-aramid fibres. Localized fibre–matrix interfacial separation and matrix cracking were also observed around the damaged yarn bundles, indicating progressive degradation of the composite structure.

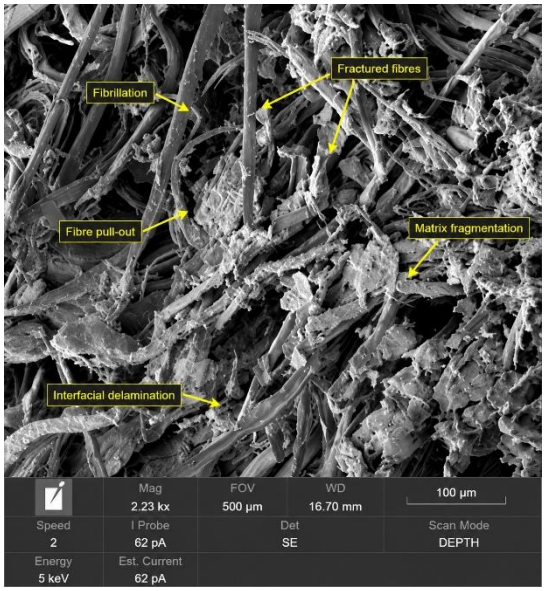


Figure 10 SEM fractography of the primary ballistic damage zone

Higher-magnification SEM observations presented in Figure 11 revealed pronounced longitudinal splitting and fibrillation of para-aramid fibres within the fractured regions. The observed fibrillar morphology was characterized by the separation of individual fibrillar structures along the fibre direction, accompanied by localized fibre rupture. These features indicate progressive damage development within the para-aramid reinforcement during ballistic loading.

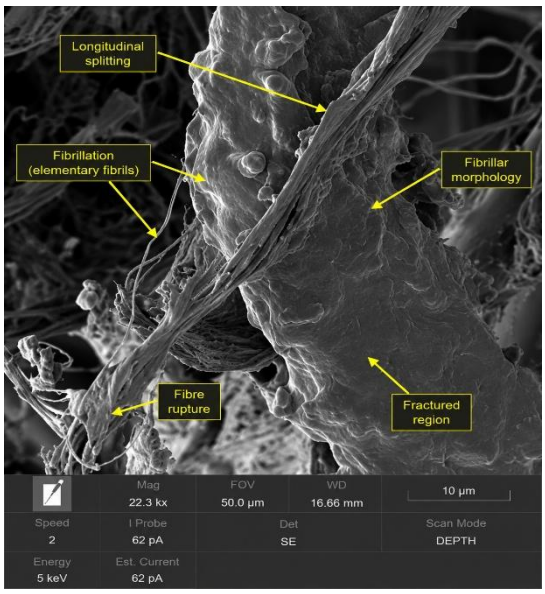


Figure 11 Fibre fibrillation and longitudinal splitting after ballistic impact

X-ray computed tomography revealed internal damage within the multilayer Twaron CT 737 composite structure following ballistic impact. The corresponding three-dimensional reconstruction is presented in Figure 12.

The reconstructed volume revealed a pronounced deformation cavity extending through several reinforcement layers beneath the impact location. Structural disruption and compaction of the woven architecture were observed along the projectile interaction region, accompanied by interlaminar separation and delamination between adjacent reinforcement layers. The internal damage extended through multiple layers without complete perforation of the composite panel.

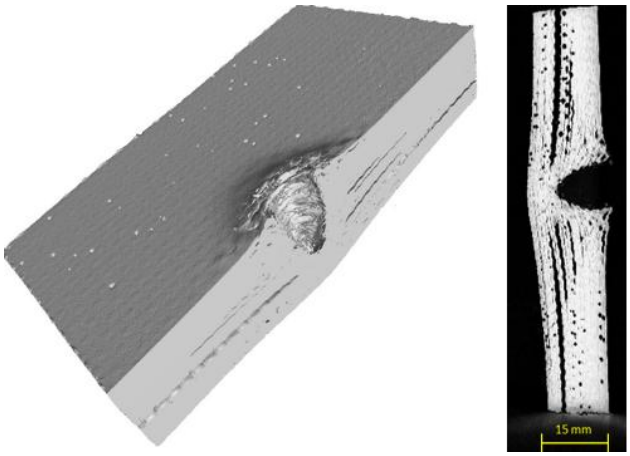


Figure 12 X-ray CT reconstruction showing internal deformation and interlaminar delamination in the Twaron CT 737 composite panel after ballistic impact

4 DISCUSSION

The ballistic experiments demonstrated that the investigated Twaron CT 737/epoxy composite panel successfully prevented complete perforation during three consecutive impacts with 9 × 19 mm FMJ projectiles. The mean impact velocity of 399.3 m/s was comparable to the reference velocity specified for the 9 mm FMJ threat under NIJ Standard 0101.06 Level II. The highest recorded impact energy reached approximately 652 J, highlighting the resistance of the multilayer woven architecture under the investigated loading conditions. Although the experimental arrangement was not designed as a complete NIJ

qualification procedure, it provided a controlled assessment of the ballistic response and associated damage evolution of the composite system.

Macroscopic observations revealed that impact-induced damage was predominantly concentrated around the projectile interaction regions, while the surrounding reinforcement retained its overall structural continuity. The spatial separation of the three impacts allowed the response of distinct locations within a single panel to be examined. Nevertheless, the available observations did not permit a definitive assessment of possible interactions between subsurface delamination zones. Consequently, the influence of preceding impacts on subsequent damage development remains uncertain. Similar mechanisms involving localized deformation and progressive stress redistribution have been reported for woven para-aramid composites subjected to ballistic loading [Rubio 2019, Signetti 2020].

The mechanical response of the investigated composite provides additional context for interpreting its ballistic behaviour. The nonlinear tensile stress–strain characteristics may be associated with progressive yarn straightening and reduction of crimp within the woven reinforcement, followed by increasing load transfer through the fibre architecture. Such deformation processes are relevant to the response of woven composites under dynamic loading, where yarn mobility and stress redistribution influence the development of localized damage [Shih 2022, Bilisik 2025]. However, the mechanical tests were performed under quasi-static conditions using laminates of different thicknesses from the ballistic panel. Therefore, the measured properties should be considered supporting material characteristics rather than direct predictors of ballistic resistance. Furthermore, the reported apparent tensile modulus may be affected by machine compliance and gripping effects because strain was determined from crosshead displacement.

SEM examination provided further insight into the microscale damage mechanisms accompanying projectile arrest. Yarn pull-out, fibre fracture, longitudinal splitting, fibrillation, matrix cracking, and localized fibre–matrix interfacial separation were observed within the damaged reinforcement. In particular, the pronounced fibrillation of para-aramid fibres suggests progressive fragmentation and separation of fibrillar structures during failure. Comparable damage morphologies have been documented in previous investigations of Twaron-based ballistic systems [Ceoromila 2025]. These observations indicate that the response of the composite involved several interacting deformation and failure mechanisms rather than a single dominant fracture process.

The CT observations complemented the fractographic findings by revealing internal deformation and interlaminar delamination extending through multiple reinforcement layers. This confirms that the damage was not limited to the visible surface regions but also involved redistribution of deformation within the laminate thickness. Similar internal damage patterns have been described in experimental and numerical investigations of multilayer ballistic composites [Nilakantan 2010, Peng 2024]. The combined SEM and CT results therefore provide a more comprehensive description of the spatial distribution of damage, linking fibre-scale fracture features with the internal structural response of the laminate.

From an engineering perspective, the principal contribution of this study lies in correlating the mechanical characteristics of the Twaron CT 737/epoxy system with its experimentally observed ballistic response and post-impact damage morphology. The successful arrest of three consecutive projectiles, together with the identification of fibre-scale and interlaminar damage mechanisms, provides useful information for evaluating the structural behaviour of multilayer para-aramid composites. The results are specific to the investigated panel configuration and loading conditions; further testing would be necessary to establish ballistic limit values or compliance with standardized body-armour qualification requirements.

Overall, the findings indicate that the ballistic response of the investigated composite was accompanied by progressive deformation and damage development across multiple structural scales. The integration of mechanical testing, ballistic experiments, SEM fractography, and X-ray computed tomography provides a consistent experimental basis for understanding the behaviour of woven para-aramid/epoxy laminates and supports their further development for ballistic protection applications.

5 CONCLUSION

The mechanical properties, ballistic resistance, and multiscale damage mechanisms of Twaron CT 737 para-aramid/epoxy composites were investigated through mechanical testing, ballistic impact experiments, scanning electron microscopy, and X-ray computed tomography. The principal findings are summarized as follows:

1) The investigated composite system exhibited a mean tensile strength of 583.1 ± 16.2 MPa and a mean flexural strength of 223.4 ± 6.3 MPa, based on seven specimens per loading configuration.
2) The 24-layer composite panel prevented complete perforation during three consecutive impacts with 9 × 19 mm FMJ projectiles. The mean impact velocity was 399.3 m/s, corresponding to a mean kinetic energy of 637.7 J. The highest recorded impact energy reached approximately 652 J.
3) Post-impact SEM observations revealed yarn pull-out, fibre fracture, fibrillation, matrix cracking, and localized fibre–matrix interfacial separation, indicating progressive damage development within the woven reinforcement.
4) X-ray computed tomography revealed internal deformation and interlaminar delamination extending through multiple reinforcement layers, demonstrating that the structural damage was not restricted to the visible impact regions.

The combined mechanical, ballistic, and microstructural observations provide a multiscale characterization of the response of Twaron CT 737/epoxy composites under ballistic loading. The successful arrest of three consecutive projectiles, together with the identification of characteristic damage mechanisms, highlights the potential of the investigated composite architecture for ballistic protection applications. Further testing under standardized conditions is recommended to assess the protective performance of the investigated composite system.

ACKNOWLEDGMENTS

The presented research was carried out within the framework of the specific research project “SV26-216” at the Department of Mechanical Engineering, University of Defence in Brno. The study was further supported by the Ministry of Defence of the Czech Republic under the institutional development programme “VAROPS (DZRO VAROPS) Military autonomous and robotic assets.”

REFERENCES

[Girma Bekele 2026] Bekele, G., Maru, D.B. and Zelelew, T.M. Advances in ballistic and impact-resistant composite fabrics: A review. Clean Energy Science and Technology, 12 March 2026. ISSN 2972-4910.

[Elgohary 2024] Elgohary, D.H. Technological aspects of body armour textiles for ballistic protection application. The Journal of The Textile Institute, 22 April 2024, Vol. 116, No. 4, pp. 535–549. ISSN 0040-5000.

[Ari 2025] Ari, A., Tekaslan, Ö., Sever, Z. and Karahan, M. Production of woven aramid based protective equipment and improving its ballistic performance. Industria Textila, 28 August 2025, Vol. 76, No. 04, pp. 591–598. ISSN 1222-5347.

[Titire 2025] Titire, L. and Muntenita, C. Ballistic Impact Study of an Aramid Fabric by Changing the Projectile Trajectory. Fibers, Vol. 13, No. 1, p. 8. ISSN 2079-6439.

[Sharma 2021] Sharma, A.P., Velmurugan, R., Shankar, K. and Ha, S.K. High-velocity impact response of titanium-based fiber metal laminates. Part I: Experimental investigations. International Journal of Impact Engineering, 2021, Vol. 152, p. 103845. ISSN 0734-743X.

[Rubio 2019] Rubio, I., Rodríguez-Millán, M., Marco, M., Olmedo, A. and Loya, J.A. Ballistic performance of aramid composite combat helmet for protection against small projectiles. Composite Structures, 2019, Vol. 226, p. 111153. ISSN 0263-8223.

[Wang 2023] Wang, Z., Zhang, H., Dong, Y., Zhou, H. and Huang, G. Ballistic performance and protection mechanism of aramid fabric modified with polyethylene and graphene. International Journal of Mechanical Sciences, 2023, Vol. 237, p. 107772. ISSN 0020-7403.

[Stojanović 2024] Stojanović, D.B., Obradović, V., Bajić, D. and Uskoković, P.S. A new generation of aramid fibers/poly (vinyl butyral) composites for ballistic protection: Recent development and advances. Journal of Engineered Fibers and Fabrics, 2024, Vol. 19. ISSN 1558-9250.

[Kondor 2025] Kondor, I.P., Líska, J. and Kovács, Z.F. Ballistic Performance of Lightweight Armor Aramid Fabric with Different Bounding Technologies. Fibers, Vol. 13, No. 8, p. 106. ISSN 2079-6439.

[Shih 2022] Shih, C.-H., You, J.-L., Lee, Y.-L., Cheng, A.-Y., Chang, C.-P. et al. Design and Ballistic Performance of Hybrid Plates Manufactured from Aramid Composites for Developing Multilayered Armor Systems. Polymers, 19 November 2022, Vol. 14, No. 22, p. 5026. ISSN 2073-4360.

[Meliande 2023] Meliande, N.M., Oliveira, M.S., Pereira, A.C., Balbino, F.D.P. and Ben-Hur da Silva Figueiredo, A. et al. Ballistic properties of curaua-aramid laminated hybrid composites for military helmet. Journal of Materials Research and Technology, 2023, Vol. 25, pp. 3943–3956. ISSN 2238-7854.

[Bilisik 2025] Bilisik, N.E., Erdogan, G. and Bilisik, K. Pull-Out Properties of Nano-Processed Para-Aramid Fabric Materials in Soft Ballistic: An Experimental Analysis. Applied Sciences, Vol. 15, No. 5, p. 2260. ISSN 2076-3417.

[Kechagiadakis 2024] Kechagiadakis, G., Lecompte, D., Van Paepegem, W., Coghe, F. and Pirlot, M. Near simultaneous multiple fragment impacts on aramid fabrics: Effects of velocity, dispersion and time intervals. International Journal of Impact Engineering, 2024, Vol. 185, p. 104830. ISSN 0734-743X.

[Chu 2024] Chu, Y., Zhu, B., Wang, X., Min, S., Chen, H. et al. Research on high-velocity ballistic impact of para-aramid sateen fabric with ZnO nanorods oriented to the development of soft body armor. Materials & Design, 2024, Vol. 248, p. 113384. ISSN 0264-1275.

[Farias-Aguilar 2021] Farias-Aguilar, J.C., Ramírez-Moreno, M.J., Gonzalez-García, D.M., Téllez-Jurado, L. and Balmori-Ramírez, H. Evaluation of the ballistic protection level of (glass-fiber reinforced polyamide 6)-aramid fabric sandwich composite panels. Journal of Materials Research and Technology, 2021, Vol. 12, pp. 1606–1614. ISSN 2238-7854.

[Viliš 2022] Viliš, J., Pokorný, Z., Zouhar, J., Vítek, R. and Procházka, J. Evaluation of ballistic resistance of thermoplastic and thermoset composite panels. Journal of Physics: Conference Series, 1 November 2022, Vol. 2382, No. 1, p. 012024. ISSN 1742-6588.

[Signetti 2020] Signetti, S., Bosia, F., Ryu, S. and Pugno, N.M. A combined experimental/numerical study on the scaling of impact strength and toughness in composite laminates for ballistic applications. Composites Part B: Engineering, 2020, Vol. 195, p. 108090. ISSN 1359-8368.

[Nilakantan 2010] Nilakantan, G., Keefe, M., Bogetti, T.A., Adkinson, R. and Gillespie, J.W. On the finite element analysis of woven fabric impact using multiscale modeling techniques. International Journal of Solids and Structures, 2010, Vol. 47, No. 17, pp. 2300–2315. ISSN 0020-7683.

[Xu 2025] Xu, Y., Zhang, H. and Huang, G. Ballistic performance of UHMWPE laminate/modified aramid fabric composite structure based on support vector machine (SVM) method. Composites Part B: Engineering, 2025, Vol. 307, p. 112855. ISSN 1359-8368.

[Peng 2024] Peng, L., Zhou, J., Wang, Q.Y., Zhang, X.F. and Guan, Z.W. Numerical modelling of the ballistic impact response of hybrid composite structures. Composites Part C: Open Access, 2024, Vol. 14, p. 100474. ISSN 2666-6820.

[Zhang 2024] Zhang, R., Song, X.-T., Zheng, B.-Q., Huang, J.-H., Deng, J. et al. Effect of hybrid strategies on the ballistic response of aramid/ultra-high molecular weight polyethylene woven fabrics. Textile Research Journal, 14 February 2024, Vol. 94, No. 11–12, pp. 1220–1232. ISSN 0040-5175.

[Ceoromila 2025] Ceoromila, A.C., Deleanu, L., Popescu, C., Lom, I., Vasiliu, A.V. et al. SEM Investigation of Failure Mechanisms in Twaron® Aramid Fibers Used for Personal Armors. Polymers, 14 April 2025, Vol. 17, No. 8, p. 1058. ISSN 2073-4360.

[Viliš 2023] Viliš, J., Vítek, R., Zouhar, J., Stejskal, M. and Neumann, V. Experimental Investigation of Armour (Armox-Aramid-UHMWPE). Manufacturing Technology, 22 December 2023, Vol. 23, No. 6, pp. 935–948. ISSN 1213-2489.

CONTACTS:
Ing. Jindrich Vilis, Ph.D.
University of Defence, Faculty of Military Technology, Department of Mechanical Engineering
Kounicova 65, 662 10 Brno, Czech Republic
jindrich.vilis@unob.cz
https://unob.cz/

LICENSE CREATIVE COMMONS:
The article is published under the terms and conditions of the Creative Commons Attribution 4.0 International License (CC BY 4.0).